Experimental characterization of the excitation state of picosecond laser-induced Tungsten plasmas

Bastien Peres, Vincent Morel, Arnaud Bultel, Abdenacer Benyagoub, Isabelle Monnet, Emmanuel Gardès, Gilles Godard, Carole Gobin, Corentin Jouen, Ammar Hideur, et al.

Experimental characterization of the excitation state of picosecond laser-induced Tungsten plasmas

Journal of Physics: Conference Series **550** (2014) 012047 doi:10.1088/1742-6596/550/1/012047

Experimental characterization of the excitation state of picosecond laser-induced Tungsten plasmas

Bastien Pérès[(1)]*, Vincent Morel[(1)], Arnaud Bultel[(1)], Abdenacer Benyagoub[(2)], Isabelle Monnet[(2)], Emmanuel Gardès[(2)], Gilles Godard[(1)], Carole Gobin[(1)], Corentin Jouen[(1)], Ammar Hideur[(1)], Ioan Schneider[(3)] and Zsolt Mezei[(3)]

[(1)]CORIA - UMR 6614 - Normandie Université, CNRS-Université et INSA de Rouen, Campus universitaire du Madrillet, 76800 Saint-Etienne du Rouvray, France
[(2)]CIMAP - UMR 6252 - CEA/CNRS/ENSICAEN/UCBN, BP 5133, 14070 Caen cedex 5, France
[(3)]LOMC - UMR 6294 - Université du Havre, 53, rue de Prony, 76058 Le Havre, France

E-mail: *bastien.peres@coria.fr

Abstract. In order to quantitatively determine the retention of light atoms by plasma facing components (mainly tungsten) used in fusion reactors, the Laser-Induced Breakdown Spectroscopy (LIBS) technique can be used. The nanosecond laser regimes classically used for LIBS present major limitations mainly due to the conditions of the laser-matter interaction process itself and cannot be used in the present context. Picosecond laser pulses are more appropriate. To validate the diagnostic based on picosecond laser pulses, preliminary characterizations of the produced plasmas have to be performed. Some related results are reported in the present communication. The study is focused on (1) the ablation of tungsten under two laser (low and high) fluence conditions and (2) the excitation equilibrium of the plasma from the nanosecond to microsecond time scales.

1. Introduction

The quantitative detection of light elements (first two lines of the periodic table of elements) trapped in heavy atoms-based matrices and their superficial gradients stay a challenge difficult to address [1]. The related measurements are required notably in the frame of the penetration of fuel in materials used in thermonuclear reactors (hydrogen and isotopes in tungsten) for safety verifications. Today, the two main techniques (NRA, Nuclear Reaction Analysis and SIMS, Secondary Ion Mass Spectrometry) used to perform such detections are based on the properties of an ionic beam impinging the surface and cannot be used in the fusion context since (1) a very low residual pressure is required and (2) the preparation of the samples is mandatory. Any *in situ* measurement is therefore impossible. Other techniques have consequently to be tested.

The Laser-Induced Breakdown Spectroscopy (LIBS) is a promising technique potentially able to measure gradients of these elements in related matrices under flexible conditions [2]. A pulsed class 4 laser beam is focused on the sample and the radiation emitted by the plasma produced by the excited ablated material is analyzed by spectroscopy. The laser pulse duration is classically of the nanosecond scale, which leads to the transient formation of a melting pool, the vaporization of which allows ionizing the atoms under irradiation until the end of the pulse.

Table 1. Nomenclature.

Symbol	Description	Unit	Symbol	Description	Unit
A_{ki}	Einstein coefficient	s^{-1}	L_{ki}	Radiance	W m^{-2} sr^{-1}
E	Energy	eV	$p(\lambda)$	Line profile	-
f	Focal length	m	t	Time	s
F_H, F_L	Fluence	J cm^{-2}	T	Temperature	K
g_i, g_k	Statistical weight	-	$[W(i)]$, $[W(k)]$	Number density	m^{-3}
$k(\lambda)$, $k_{\lambda_{ki}}$	Absorption coefficient	m^{-1}	δ	Plasma diameter	m
$L_{ki,\lambda}(\lambda)$	Spectral radiance	W m^{-2} sr^{-1} m^{-1}	λ	Wavelength	m

Despite its promising aspect, the nanosecond LIBS technique presents major limitations arising mainly from the conditions of the laser-matter interaction process itself leading to an initial departure from equilibrium [3], a strong initial continuum [4] and the melting pool formation [5]. The exploitation of ultra-short (picosecond and femtosecond) pulses in LIBS is very promising from this point of view. Indeed, the pulse energy is totally transferred to the sample owing to its briefness and distributed with almost the same probability to all elements over the pulse penetration depth (much lower than in nanosecond regime). It is particularly appropriate to the analysis of samples composed with elements of very different atomic mass and especially for light elements in heavier matrices. The continuum intensity is reduced at early times, which is particularly appropriate to the observation of early lines due to light elements. The detection limits should be strongly lowered while the capacity of depth-profiling should be strongly improved.

Since the energy available per pulse is higher in picosecond regime than in femtosecond regime for compact sources, we have implemented in our LIBS platform a picosecond laser source. This will help to a future implementation on a fusion reactor in a semi-industrial environment and enlarge the room for manoeuvre. Preliminary tests are performed on tungsten without retention of light elements. These tests are described and analyzed in the upcoming sections. After description of the LIBS platform used to analyze radiation emitted by the laser-induced plasma, results on ablation craters are first given. Two (low and high) fluence conditions are tested. Using relevant calibrations, excited states number density is determined and the Boltzmann plots are derived. The concept of excitation temperature is introduced and discussed in the light of the present results. In particular, the relevance of the McWhirter criterion is discussed.

2. The CORIA's LIBS platform

The CORIA's LIBS platform is displayed on figure 1. After several mirrors, the picosecond laser pulse provided by an EKSPLA source (532 nm, 30 ps, 10 mJ) is focused with a converging lens (5 cm or 50 cm in focal length) on a tungsten sample located on a rotating plate inside a chamber, the ultimate pressure of which is 0.4 Pa. Two lenses providing a magnification of 2 are used to collect a part of the light emitted by the resulting plasma toward an Ebert-Fastie spectrometer (f = 2 m in focal length, aperture of $f/15$) on the exit slit of which an ICCD camera Roper Scientific PIMAX 2 (512×512 $pixels^2$) is connected. The spectroscopic device allows a spectral resolution of around 5×10^{-2} nm in the visible spectral range.

The craters formed during the laser-matter interaction are observed using a calibrated microscope, the maximum magnification of which is 50. The calibration is performed with wires of known diameter. The crater diameter can be determined with an accuracy of ± 20 μm. The spectroscopic analysis is performed using the WinSpec software with a gate Δt of 50 or 100 ns between $t = 0$ (the time at which the laser pulse reaches the sample) and $t_{max} = 2$ μs. The calibration allowing the conversion from signals in arbitrary units to spectral radiance is performed with a tungsten ribbon lamp at T_c = 2475 K ± 5 K. The entrance slit of the

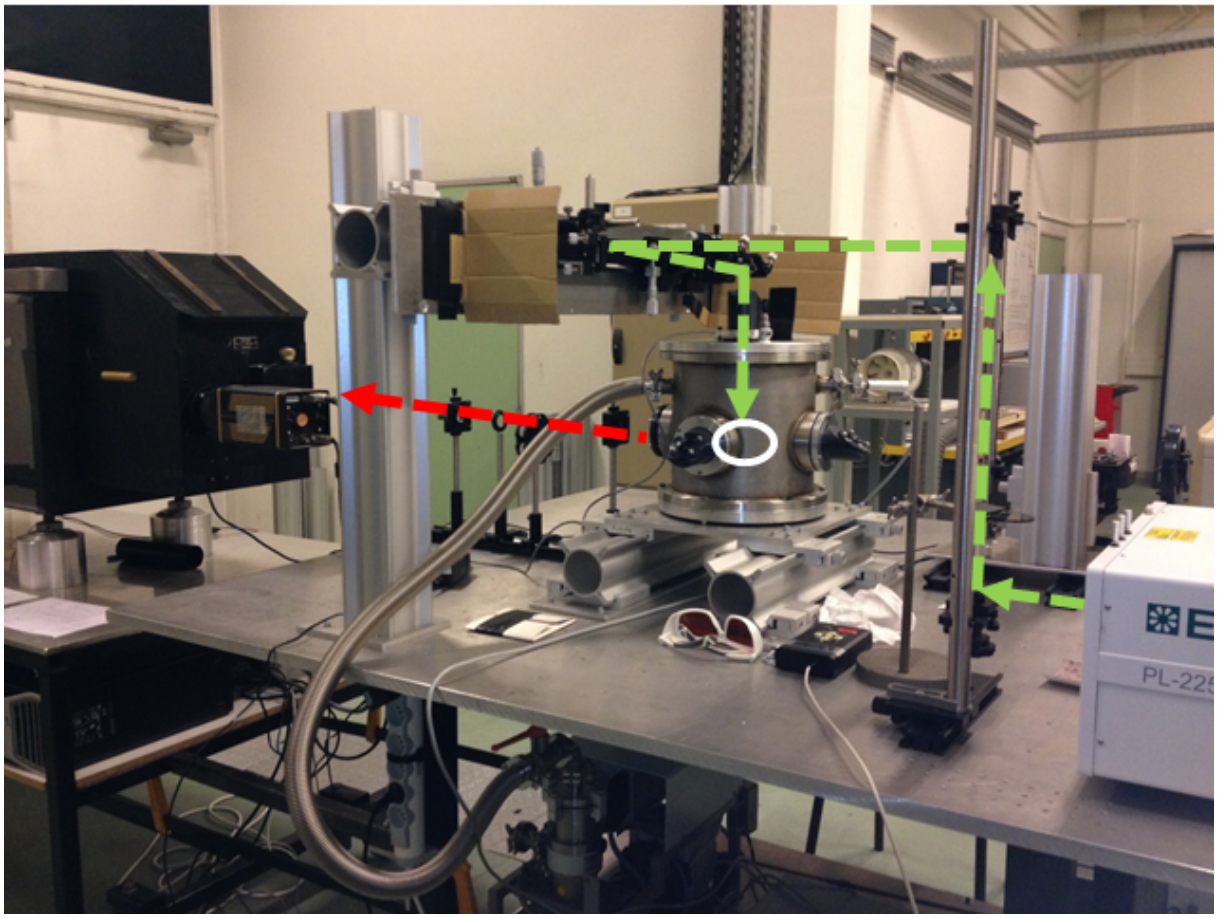

Figure 1. The CORIA's LIBS platform. The EKSPLA laser source (on the right) emits light pulses along the green trajectory. After several mirrors, a converging lens focuses the pulse on a horizontal sample located inside the central chamber. A part of the light emitted by the laser-induced plasma is then collected by two lenses along the red optical axis toward a spectrometer (on the left) equipped on its exit slit with an ICCD camera connected to a computer. The spectral analysis is finally performed.

spectrometer is fixed at 100 μm (Δx = 50 μm for the detection volume width within the plasma) and the optical axis-sample distance is z = 650 μm. The detection volume height is Δz = 1.3 mm.

3. Ablation craters

Two series of experiments have been performed in low fluence (LF) and high fluence (HF) conditions using the two lenses mentioned above. The first condition corresponds to F_L = 10 J cm^{-2} and the second condition to F_H = 1000 J cm^{-2}. Table 2 reports the mean characteristics obtained for the craters for these two fluence conditions. It is interesting to note that an increase in the irradiance of a factor of 100 leads to a similar increase of the ablation rate. Since this increase results from light more focused on the sample, the ablation diameter is consequently reduced, but by a factor of 5 only. The ablated volume (and therefore the ablated atoms) is increased by a factor of 4 when the fluence is increased from F_L to F_H.

This is a very interesting result from the LIBS diagnostic point of view. Despite a strong

Table 2. Mean characteristics of the craters obtained under low (LF) and high (HF) fluence conditions with the picosecond laser source of the CORIA's LIBS platform.

Characteristic	LF conditions (F_L = 10 J cm^{-2}) (over 1000 pulses)	HF conditions (F_H = 1000 J cm^{-2}) (over 200 pulses)
Ablation rate	10 nm pulse^{-1}	1 μm pulse^{-1}
Ablation diameter	750 μm	150 μm
Ablated volume	4.4×10^{-15} m^3 pulse^{-1}	1.8×10^{-14} m^3 pulse^{-1}
Ablated atoms	2.8×10^{14} pulse^{-1}	1.1×10^{15} pulse^{-1}

increase in the fluence of a factor of 100, the ablated atoms number can be considered as relatively constant. A too strong focus of the laser light on the sample leads only to a reduction of the spatial resolution which can question the ability of the technique to provide precise depth profiling measurements if gradients with characteristic length scales lower than 1 μm are expected for the material to be tested.

4. Spectroscopic analysis

The tungsten spectroscopy faces the problem of the lack of basic data concerning mainly the Einstein coefficient A_{ki} of the radiative transitions. As an example, the different lines of W I reported with their Einstein coefficient in the NIST database [6] represents only 7 % of the total of the reported lines. The database is therefore far to reach the 25 % reported lines of Fe I with their Einstein coefficient, which is also far from the 98 % obtained for N I. In addition, the transitions with the corresponding Einstein coefficient are only around 500 for W I whereas they are around 2500 for Fe I. The quantitative analysis of spectra emitted by the laser-induced plasmas requires the Einstein coefficient. As a result, the number of lines involved in the analysis is small. In addition, the W ionization limit is relatively low (E_{ion} = 7.864 eV). The lower level of a radiative transition in the visible spectral range has therefore a high probability to be energetically close to the ground state and to be self-absorbed. A relevant way to reduce this probability is to use transitions, the Einstein coefficient of which is not too high. But in this case, the spectral radiance is also reduced and can prevent a satisfactory observation of the lines. The choice of the transitions finally retained for the analysis is therefore the result of a compromise between all these aspects. They are listed in table 3 with their characteristics. Only W I transitions have been observed.

Figure 2 displays an example of the calibrated spectra which can be observed under HF conditions. In particular, this figure shows the evolution in time of the spectra over the spectral range 504.6 nm $< \lambda <$ 509.6 nm for t = 150, 250, 650 and 1050 ns. The initial continuum is easily observed even if its spectral radiance is moderate and clearly lower than the one of the lines. For a given observation time, this continuum increases with the wavelength. This indicates that the plasma electron temperature is moderate if we consider the initial cooling mainly due to the radiative recombination. The resulting continuum is then emitted in the near infrared spectral region. The group of lines at λ = 507.1515 nm presents a very interesting behavior. These lines overlap with a relative contribution varying in time. As a result, this group is not symmetric and presents a time-dependent redshift. As far as we know, their Stark broadening and shift parameters have not yet been reported in literature.

The radiance L_{ki} (see Table 1 for the units of variables used in the present paper) of each $k \rightarrow i$ line of table 3 is calculated from

$$L_{ki} = \int_0^{+\infty} L_{ki,\lambda}(\lambda) d\lambda \qquad [\mathrm{W\,m^{-2}\,sr^{-1}}] \tag{1}$$

Table 3. W I radiative transitions used for the picosecond laser-induced plasmas analysis.

Wavelength	Einstein	Lower state		Upper state		Time of
	coefficient	Energy	Degeneracy	Energy	Degeneracy	observation
λ_{ki} (nm)	A_{ki} (s^{-1})	E_i (eV)	g_i	E_k (eV)	g_k	t (ns)
449.2298	3.60×10^5	2.121	9	4.880	11	200
449.3958	2.80×10^6	2.387	5	5.145	7	200, 600, 1000
449.4497	3.00×10^6	2.387	9	5.145	7	100, 200, 600, 1000
449.5294	3.30×10^5	1.868	11	4.626	11	600, 1000
450.4838	7.00×10^5	1.508	9	4.259	7	100, 200, 600, 1000
451.7344	3.50×10^6	2.266	5	5.010	3	600, 1000
498.2593	4.17×10^5	0.000	1	2.488	3	200, 600, 1000
498.4698	9.00×10^5	2.352	7	4.839	5	600, 1000
498.6920	6.30×10^5	1.868	11	4.354	9	100, 200, 600, 1000
500.6150	1.20×10^6	0.771	9	3.247	7	100, 200, 600, 1000
501.5304	5.40×10^5	0.599	7	3.070	9	100, 200, 600, 1000
504.0360	5.20×10^5	1.650	3	4.109	5	200, 600, 1000
505.2230	1.10×10^6	2.602	5	5.055	3	100, 200, 600, 1000
505.3276	1.90×10^6	0.210	3	2.660	3	100, 200, 600, 1000
505.4596	3.30×10^5	0.210	3	2.660	5	100, 200, 600, 1000
505.5516	4.00×10^6	2.787	9	5.239	7	1000
507.1515	3.40×10^5	2.436	13	4.880	11	100, 200, 600, 1000
511.7612	1.61×10^5	2.458	11	4.880	11	600, 1000
512.4234	4.00×10^5	1.857	5	4.276	5	200, 600, 1000
514.5774	2.10×10^6	2.602	5	5.010	3	200, 600, 1000
515.9095	9.10×10^3	1.857	5	4.259	7	1000
518.3965	9.60×10^5	2.353	7	4.744	9	100, 200, 600, 1000
520.4520	6.80×10^6	2.533	3	4.914	3	100, 200, 600, 1000
520.6180	2.49×10^6	2.458	7	4.839	5	200, 600, 1000
522.4657	1.20×10^6	0.588	7	2.971	5	100, 200, 600, 1000
524.2980	1.10×10^6	2.037	9	4.401	7	100, 200, 600, 1000
524.7417	3.00×10^4	1.868	11	4.231	9	100, 200, 600, 1000
525.4542	3.86×10^5	1.917	7	4.276	5	200, 600, 1000
525.5396	2.61×10^6	2.787	9	5.145	7	200, 600, 1000
526.8550	1.40×10^5	2.121	9	4,474	9	600, 1000
547.7776	2.60×10^5	1.181	1	3.444	3	200, 600, 1000
549.6234	4.00×10^5	2.787	9	5.042	7	200, 600
550.0490	6.90×10^5	2.458	11	4.712	9	200, 600, 1000
551.4976	7.30×10^5	0.412	5	2.660	3	100, 200, 600, 1000
582.2600	1.07×10^6	2.787	9	4.916	7	200, 600
644.5120	6.40×10^5	2.353	7	4.276	5	200, 600, 1000

The influence of the stimulated emission can be neglected. Therefore, the spectral radiance $L_{ki,\lambda}(\lambda)$ can be written as

$$L_{ki,\lambda}(\lambda) = \frac{2\,h\,c^2}{\lambda_{ki}^5}\frac{[W(k)]}{[W(i)]}\frac{g_i}{g_k}\left(1-e^{-k(\lambda)\delta}\right) \qquad [\mathrm{W\,m^{-2}\,sr^{-1}\,m^{-1}}] \tag{2}$$

where $k(\lambda)$ (in $\mathrm{m^{-1}}$) is the absorption coefficient per unit length at the wavelength λ, and $[W(k)]$ and $[W(i)]$ are the mean number density over the plasma diameter δ of the upper and lower

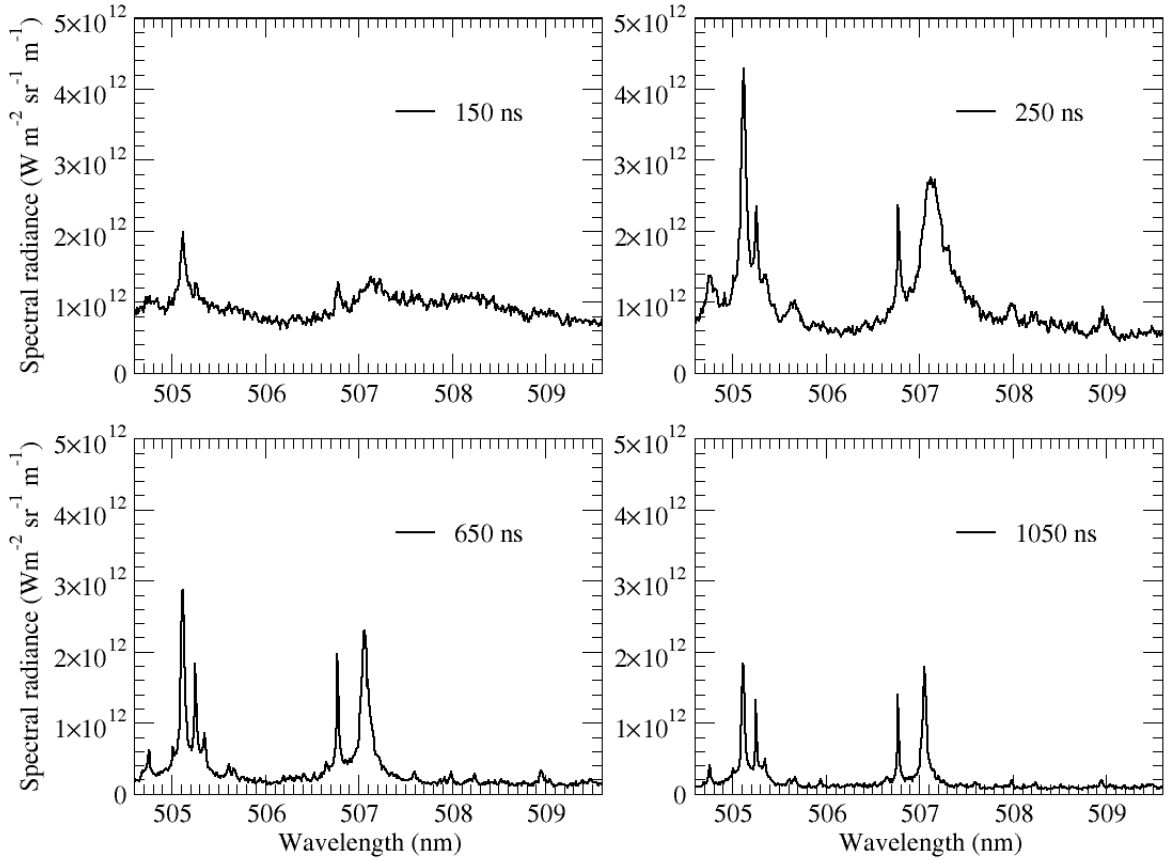

Figure 2. Spectra observed for a gate of $\Delta t = 100$ ns at time $t = 150$, 250, 650 and 1050 ns over the spectral range 504.6 nm $< \lambda <$ 509.6 nm.

states of the transition, respectively. The absorption coefficient depends on the line profile $p(\lambda)$ such as $k(\lambda) = k_{\lambda_{ki}}\, p(\lambda)$ where

$$k_{\lambda_{ki}} = \frac{A_{ki}\,\lambda_{ki}^4}{8\,\pi\,c}\,[W(i)]\,\frac{g_k}{g_i}\,\frac{1}{\int_0^{+\infty} p(\lambda)\,d\lambda} \qquad [\mathrm{m}^{-1}] \tag{3}$$

is the absorption coefficient at the line center. Therefore

$$L_{ki} = \frac{2\,h\,c^2}{\lambda_{ki}^5}\,\frac{[W(k)]}{[W(i)]}\,\frac{g_i}{g_k}\int_0^{+\infty}\left(1 - e^{-k_{\lambda_{ki}}\,p(\lambda)\,\delta}\right)d\lambda \tag{4}$$

If

$$e^{-k_{\lambda_{ki}}\,p(\lambda)\,\delta} \simeq 1 - k_{\lambda_{ki}}\,p(\lambda)\,\delta \tag{5}$$

the transition is optically thin and

$$L_{ki} \equiv \frac{2\,h\,c^2}{\lambda_{ki}^5}\,\frac{[W(k)]}{[W(i)]}\,\frac{g_i}{g_k}\,k_{\lambda_{ki}}\,\delta\int_0^{+\infty} p(\lambda)d\lambda \tag{6}$$

In case of Doppler ($type \equiv$ D) or Lorentz ($type \equiv$ L) broadening, we have

$$\int_0^{+\infty} p(\lambda) d\lambda = a_{type}\, \Delta\lambda_{1/2} \qquad [\mathrm{m}] \tag{7}$$

where $\Delta\lambda_{1/2}$ is the Full Width at Half Maximum (FWHM) of the line and $a_D = \sqrt{\frac{\pi}{4 \ln 2}}$ and $a_L = \frac{\pi}{2}$. The radiance of the line is then

$$L_{ki} = \frac{2\, h\, c^2}{\lambda_{ki}^5} \frac{[W(k)]}{[W(i)]} \frac{g_i}{g_k} k_{\lambda_{ki}} \delta\, a_{type}\, \Delta\lambda_{1/2} \tag{8}$$

With (3), we obtain

$$L_{ki} = \frac{h\, c}{\lambda_{ki}} [W(k)] \frac{A_{ki}}{4\pi} \delta \tag{9}$$

The condition (5) is fulfilled if

$$k_{\lambda_{ki}}\, p(\lambda)\, \delta < k_{\lambda_{ki}}\, \delta \leq 0.1 \tag{10}$$

From the absorption coefficient definition (3), we deduce the condition for an optically thin transition

$$[W(i)] \leq [W_{ki}^0(i)] = 0.1\, \frac{8\, \pi\, c\, a_{type}\, \Delta\lambda_{1/2}}{A_{ki}\, \lambda_{ki}^4\, \delta} \frac{g_i}{g_k} \qquad [\mathrm{m}^{-3}] \tag{11}$$

If the previous condition is not fulfilled, radiation can be considered as partially self-absorbed. In order of magnitude, data reported in table 3 lead to $[W_{ki}^0(i)] \simeq 10^{22}$ m^{-3}.

We calculate the upper state number density by assuming (α) the related radiative transition optically thin and (β) a constant diameter δ for the plasma. Actually, this diameter evolves with time due to the plasma expansion over the observation time. Nevertheless, we have considered in a first approximation that this increase is moderate around $\delta = 200$ μm, the value of which is confirmed by direct imagery. This value is very close to the crater diameter obtained under HF conditions. The number density (in m^{-3}) is therefore derived from equation (9) leading to

$$[W(k)] = \frac{4\pi L_{ki}}{A_{ki}\delta} \frac{\lambda_{ki}}{hc} \tag{12}$$

which is used for the determination of the upper state number density.

Table 3 reports the time at which the studied lines can be observed. Even low Einstein coefficient transitions can be detected. Figure 3 shows the Boltzmann plot for t = 150, 250, 650 and 1050 ns derived from the upper state number density therefore obtained. A large part of the lower states of the involved transitions have an energy higher than 2 eV. For them, the Boltzmann plots display a number density much lower than the limit (11) estimated here to $[W_{ki}^0(i)] \simeq 10^{22}$ m^{-3}: as a result, most of the transitions can be considered as optically thin. We can observe that the order of magnitude of the density levels are relatively constant. For each boltzmann plot we performed a linear interpolation with the least squares method. The slope of this interpolation lines is directly proportional to the excitation temperature. Despite the dispersion resulting from the different experimental uncertainties, the determination of which will be shortly performed, the excitation temperature defined as [7]

$$T_{exc} = -\frac{1}{k_B \left[\frac{d}{dE_k} \left(\ln([W(k)]/g_k)\right)\right]_{lsl}} \qquad [\mathrm{K}] \tag{13}$$

is derived.

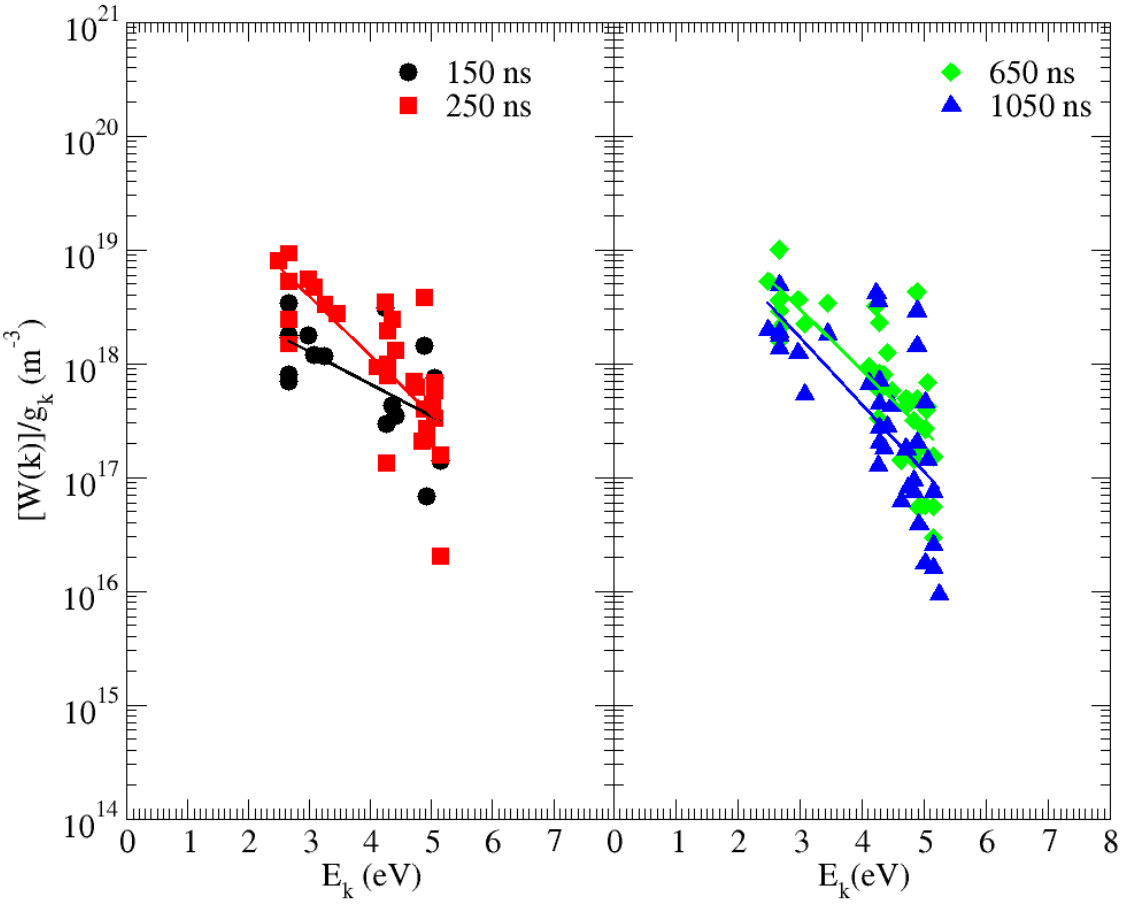

Figure 3. Boltzmann plot obtained at t = 150, 250, 650 and 1050 ns. The straight lines correspond to the least squares line for each time.

Figure 4 shows the temporal evolution of the excitation temperature obtained from the four Boltzmann plot interpolation lines. First, at early times between 150 ns and 250 ns after the plasma pulse, T_{exc} abruptly decreases from 18000 K to 9000 K. Then from this time until 1050 ns, T_{exc} decreases slightly and stabilizes at $\sim$ 9000 K. This indicates that the plasma seems to reach an excitation quasi-steady state. The order of magnitude obtained for T_{exc} needs to be confirmed as well as its uncertainty. Moreover, the dynamics at early times must be further study despite the absence of observable lines in spectra. From this point of view, deriving electron density and temperature from the continuum emitted at early tiles could provide valuable information on the coupling between electron and excitation temperatures. Nevertheless, the global behavior of this experimentally determined excitation temperature seems similar to the one observed on nanosecond laser-induced tungsten plasmas [8].

5. Conclusion

In conclusion, we have given an insight into the dynamics of the excitation state of a picosecond laser-induced tungsten plasma through the experimental determination of the excited states number density and the excitation temperature. As a first observation, the global behavior and the order of magnitude of this two quantities are close to values reported in literature in

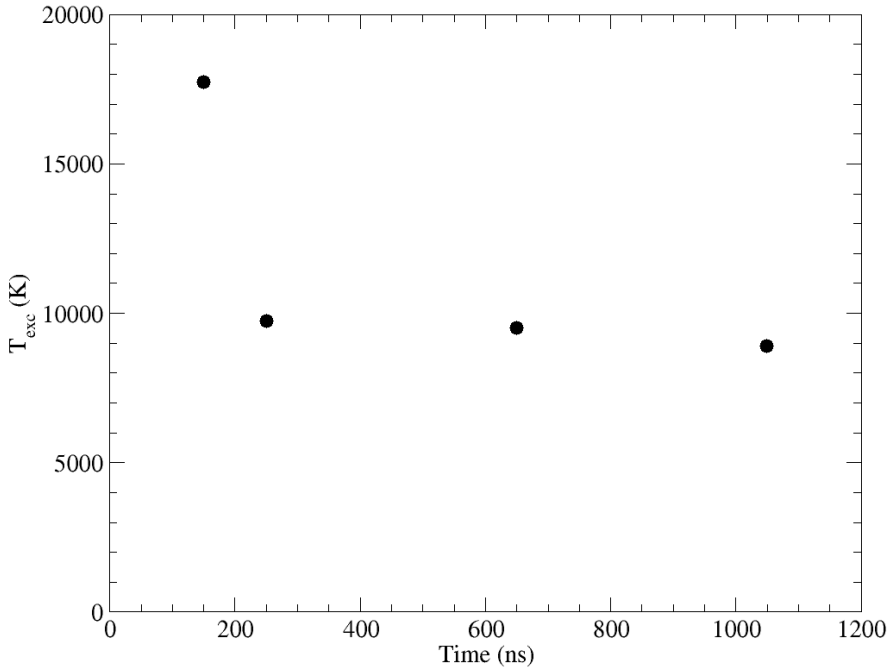

Figure 4. Excitation temperature obtained at t = 150, 250, 650 and 1050 ns.

nanosecond regime. However, the measurements were performed considering spatially averaged quantities. Our next two objectives are to improve the resolution in space and time by performing (1) simultaneous measurements at different locations perpendicularly to the sample surface and (2) additional measurements over the time interval [0,250] ns.

References

[1] Khater M A 2013 *Optics and Spectroscopy* **115** pp 574-590
[2] Hahn D W and Omenetto N 2012 *Applied Spectroscopy* **66** pp 347-419
[3] Elhassan A, Giakoumaki A, Anglos D, Ingo G M, Robbiola L and Harith M A 2008 *Spectrochim. Acta B* **63** pp 504-511
[4] Sirven J-B, Bousquet B, Canioni L and Sarger L 2004 *Spectrochim. Acta B* **59** pp 1033-1039
[5] Leggieri G, Luches A, Martino M, Perrone A, Majni G, Mengucci P and Mihailescu I N 1995 *Thin Solid Films* **258** pp 40-45
[6] *http* : *//physics.nist.gov/PhysRefData/ASD/levels_form.html*
[7] Morel V and Bultel A 2014 *Spectrochim. Acta B* **94-95** pp 63-70
[8] Farid N, Li C, Wang H and Ding H 2013 *J. Nucl. Mat.* **433** pp 80-85